Journal of Fluorescence
https://doi.org/10.1007/s10895-024-03849-9

RESEARCH

Vitamin B_6 Cofactor Pyridoxal 5′-phosphate Conjugated Papain-Stabilized Fluorescent Gold Nanoclusters for Switch-on Detection of Zinc(II)

Jayant Chaudhary[1] · Aditi Tripathi[1] · Suban K. Sahoo[1]

Received: 23 May 2024 / Accepted: 15 July 2024
© The Author(s), under exclusive licence to Springer Science+Business Media, LLC, part of Springer Nature 2024

Abstract

In this study, fluorescent gold nanoclusters (AuNCs) conjugated with pyridoxal-5-phosphate (PLP) were synthesized, characterized, and used for Zn^{2+} fluorescence turn-on sensing. PLP was conjugated over the surface of papain-stabilized fluorescent gold nanoclusters (pap-AuNCs; $\lambda_{ex}=380$ nm, $\lambda_{em}=670$ nm) by forming imine linkage. Due to this modification, the red color emitting pap-AuNCs changed to orange color emitting nanoclusters PLP_pap-AuNCs. The nano-assembly PLP_pap-AuNCs detect Zn^{2+} selectively by showing a notable fluorescence enhancement at 477 nm. Zn^{2+} detection with PLP_pap-AuNCs was quick and easy, with an estimated detection limit of 0.14 µM. Further, paper strips and cotton buds coated with PLP_pap-AuNCs were developed for affordable on-site visual detection of Zn^{2+}. Finally, the detection of Zn^{2+} in actual environmental water samples served as validation of the usefulness of PLP_pap-AuNCs.

Keywords Fluorescent gold nanoclusters · Fluorescence sensor · Vitamin B6 cofactor · Pyridoxal-5'-phosphate · Zn(II)

Introduction

Fluoro-sensors for detecting physiologically active metal ions and their applications in material, environmental, and biological sciences are continually expanding. The growth of fluorescence sensors for the qualitative and quantitative detection of biospecies has piqued the interest of supramolecular and analytical chemists due to the several benefits, including high selectivity, sensitivity, cost-effectiveness, ease of handling, low detection limit, and on-site real-time monitoring without the use of sophisticated equipments [1–5]. Fluorescent chemosensors comprise mainly two major components, i.e., a light-emitting group (fluorophore) and a recognition site. Due to mechanisms such as photo-induced electron transfer, excimer formation, fluorescence resonance energy transfer, internal charge transfer, C = N isomerization, and others, when the target analyte selectively interacts with the recognition site, the optical property of the fluorophore is disturbed, leading to a shift, quenching, or amplification in the initial fluorescence signal of the sensor (6–7). In the last few decades, a variety of fluorescent sensors have been reported using organic dyads and fluorescent nanomaterials to detect metal ions, anions, and neutral molecules.

Transition metal cations like Zn^{2+}, $Fe^{3+/2+}$, Co^{2+}, Cu^{2+}, etc., are essential for the normal functioning of metabolic processes. However, they are detrimental at large concentrations and pose a hazard to human health via cellular toxicity, liver damage, and neurological illnesses. (8–9) Like other transition metal ions, Zn^{2+} has received significant interest due to its biological role. Zinc is the second most prevalent and vital transition element in the human body. It regulates enzymes, acts as a physical cofactor in metalloproteins, transmits neural activity, and is responsible for regulating gene expression and plenty of other biological functions. Zn^{2+} mediated bio compounds are widely used in medical treatment as tumor photosensitizers, antimicrobial, antioxidant agents, and radioprotective agents [10–13]. On the other side, excess Zn^{2+} ion leads cellular processes to become unbalanced, resulting in neurological disorders including Alzheimer's disease, Menkes and Wilson diseases, Parkinson's disease, prostate cancer, and diabetes

✉ Suban K. Sahoo
sks@chem.svnit.ac.in

1 Department of Chemistry, Sardar Vallabhbhai National Institute Technology, Surat, Gujarat 395007, India

Published online: 23 July 2024

[14–16]. In addition, high levels of zinc in the environment may diminish soil microbial activity, resulting in phytotoxicity. As a result, there is significant research on developing fluorescence sensors for rapid and selective detection of Zn^{2+} in biological and environmental systems, especially in the presence of interfering metal ions with similar coordination behaviour like Cd^{2+}. Also, Zn^{2+} is diamagnetic in nature, and therefore it does not produce any magnetic or spectroscopic signals, making it impossible to detect in biological processes using standard analytical techniques like electron paramagnetic resonance (EPR) spectroscopy or nuclear magnetic resonance (NMR), Mossbauer spectroscopy. [17–22] So, fluorescence spectroscopy has been chosen as an ideal and convenient approach for detecting Zn^{2+} in biomolecules at the authentic site.

Vitamin B_6 (VB_6) cofactors comprise a set of six water-soluble chemically related molecules with a pyridine ring at its centre, i.e., pyridoxamine (PYOA), pyridoxal (PL), pyridoxine (PN), and their monophosphorylated derivatives. [23] Pyridoxal-5'-phosphate (PLP) is the most active form of VB_6 cofactors. These cofactors are essential in various biochemical activities, such as decarboxylations of aminoacid [24], racemization [25], and enzymatic and non-enzymatic transformations. [26–28] In animals and plants, VB_6 aids in the manufacture of fatty acids, the breakdown of some storage compounds, and the biosynthesis of plant neurotransmitters, hormones, and organelle-specific chemicals like chlorophyll [29–31]. VB_6 deficiency is frequently associated with dermatitis, microcytic anemia, or electroencephalographic abnormalities. Immune system dysfunction, convulsive seizures, depression, and confusion have also been reported (32–33). The United States Food and Nutrition Board of the Institute of Medicine recommends dietary allowances (RDA) for VB_6 ranging from 1.3 mg (young adults) to 1.7 mg (adult males), with lactating women up to 2 mg. Nonetheless, a few case studies have been published in which high doses of the vitamin cause neurological disorders because VB_6 participates in so many biochemical pathways, and also abnormal levels of VB_6 cofactors, particularly PLP and pyridoxal, can be harmful to human health [34–38]. As a result, there is much interest in developing new methods for detecting and monitoring the VB_6 cofactor PLP.

Due to their discrete energy levels, noble metal nanoclusters (NCs) have unique photophysical and chemical properties that make them useful for a variety of applications, including catalysts, sensing, and cell labelling (39–40). In these domains, NCs based on gold (Au) and silver (Ag) have been widely used. Gold nanoclusters, which are made up of a few hundred to several thousand Au atoms, have remarkable optical characteristics, [41] such as strong fluorescence, good photostability, and biocompatibility [42, 43]. They also show intense fluorescence. The primary determinant of the fluorescence characteristics of gold nanoclusters is the Au core, which experiences a radiative transition due to metal-metal interaction. Furthermore, the surface ligands are important because they influence the fluorescence properties via mechanisms including ligand-to-metal charge transfer (LMCT) and/or ligand-to-metal-metal charge transfer (LMMCT) [44]. Here, a fluorescent gold nanocluster stabilised by papain that emits red light (pap-AuNCs) was synthesized and post-functionalized with PLP to create the nanoprobe PLP_pap-AuNCs (Scheme 1). The development of PLP_pap-AuNCs led to the modification in fluorescent color from red to orange, which allowed the detection of PLP using pap-AuNCs as a nanoprobe. Subsequently, the orange-emitting PLP_pap-AuNCs were used for the fluorescent turn-on sensing of Zn^{2+} in an aqueous medium.

Experimental

Reagents and Instruments

The analytical grade NaOH and metal salts such as $CaCl_2$, $HgCl_2$, $Fe(NO_3)_3{\cdot}9H_2O$, $ZnCl_2$, $MgCl_2{\cdot}6H_2O$, $Cr(NO_3)_3{\cdot}9H_2O$, $MnCl_2{\cdot}4H_2O$, $CdCl_2.2H_2O$, $NiCl_2{\cdot}6H_2O$, $PbCl_2$, $FeSO_4{\cdot}7H_2O$, $Al(NO_3)_3{\cdot}9H_2O$ were provided by Rankem and Finar Pvt. Ltd, India. $HAuCl_4.4H_2O$, papain (pap), and various VB_6 cofactors (PY, PN, PLP, and PYOA) were procured from Sigma-Aldrich. Stock solutions of various analytes (1 mM) and EDTA (1 mM) were made with double-distilled water and utilised following appropriate dilution.

An Agilent Technologies Cary Eclipse fluorescence spectrophotometer was used to perform fluorescence spectral measurements with both the excitation and emission slit widths set at 10 nm, and the solution containing the nanoclusters was excited at a wavelength of 380 nm. UV-visible absorption spectra were obtained using the Varian Cary 50 spectrophotometer. A quartz cuvette with a 1 cm path length was used for recording the spectra. With a HORIBA SZ-100, dynamic light scattering (DLS) data was obtained.

Synthesis of pap-AuNCs

The reported method was adopted to prepare AuNCs stabilized with papain (pap-AuNCs) [45]. Initially, 2.5 mL of $HAuCl_4$ solution (10 mM) and 2.5 mL of papain solution (50 mg/mL) were thoroughly mixed at room temperature via vigorous mixing. Subsequently, the mixture was incubated at 90 °C for 5 min. Following this, 0.8 mL of NaOH solution (1.0 M) was added to the sample solution and further incubated for an additional 15 min. The color of the

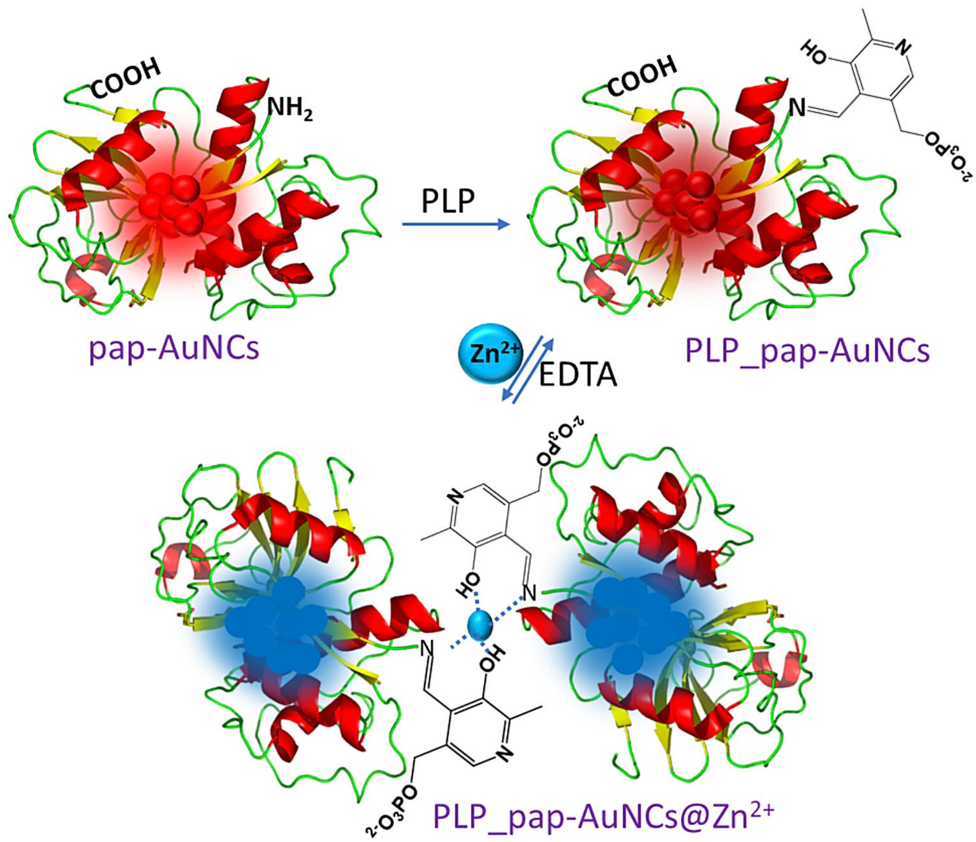

Scheme 1 Schematic representation for the change in fluorescence of Papain-AuNCs for the relay detection of PLP and Zn^{2+}

mixture changed to yellow, indicating the formation of pap-AuNCs. The purified pap-AuNCs solution via dialysis was kept at 4 °C for later studies.

Sensing Procedure

From the stock, 100 µL of pap-AuNCs was diluted to 2 mL with water to prepare the nanoclusters' working solution. In order to examine the interactions with VB_6 cofactors, 100 µL of pap-AuNCs was mixed with 100 µL of 1 mM VB_6 cofactors, and then diluted to 2 mL using water. Significant changes in fluorescence emission were seen when PLP was added to pap-AuNCs. An emission band appeared at 525 nm, and concomitantly quenched at 700 nm. These alterations were indicative of the development of PLP_pap-AuNCs. The PLP_pap-AuNCs fluorescence emission spectra were evaluated by adding several metal ions (100 µL, 1.0 mM), including Zn^{2+}, Mg^{2+}, Pb^{2+}, Ni^{2+}, Mn^{2+}, Hg^{2+}, Ca^{2+}, Al^{3+}, Cd^{2+}, Fe^{3+}, Fe^{2+}, and Cr^{3+}. The competitive experiments were carried out by recording the fluorescence of PLP_pap-AuNCs in the presence of Zn^{2+} (100 µL, 1.0 mM) and other interfering metal ions at equimolar concentrations. The method used for fluorescence titration involved successive addition of Zn^{2+} ions to the nanoprobe incrementally. The limit of detection (LOD) was computed using the slope of the calibration curve using the IUPAC-approved formula, which is LOD = 3σ/slope, where σ is the relative standard deviation (RSD) of 10 blank measurements.

To conduct recovery experiments in real samples, river water from the Tapi River, Surat, India, and tap water from the laboratory were collected and filtered using Whatman filter paper to eliminate any particulate matter. Initially, the samples of water were added directly to the nanoprobe solution. No discernible alterations in the fluorescence spectra of the probe were observed. Therefore, to assess the feasibility of the developed nanoprobe for practical applications, a known concentration of Zn^{2+} solution from its standard solution was poured into the water samples. The poured water samples were then added to the probe solution. The resulting change in the fluorescence spectra was used to estimate the concentration of Zn^{2+} in the real water samples. This approach allows for the evaluation of the nanoprobe performance in real-world scenarios and provides insight into its potential for practical applications in environmental monitoring or water quality assessment.

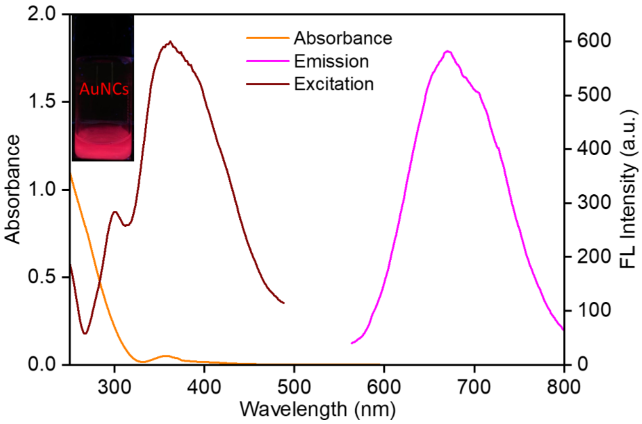

Fig. 1 Fluorescence emission ($\lambda_{ex}=380$ nm), excitation ($\lambda_{em}=670$ nm) and UV-Vis absorption spectra of pap-AuNCs (inset showed the fluorescent vial of pap-AuNCs under UV light)

Results and Discussion

Synthesis of pap-AuNCs

Proteins are useful biocompatible stabilizers to obtain fluorescent metal nanoclusters. Papain, an endolytic cysteine protease is extracted from latex of Carica papaya. It is a single polypeptide chain with 212 amino acid residues, some of which are cysteine, histidine, and asparagine. Through vigorous stirring of a mixture of $HAuCl_4$ and papain under a basic medium at 90 °C for 15 min, pap-AuNCs were synthesized facilely. [46] According to reports, the sulfhydryl group of cysteine residues is essential for promoting the Au-S bond-mediated pap-AuNC synthesis. Studies also revealed that certain amino acid residues were more likely to take part in hydrogen bonding and polar interactions to regulate the growth of pap-AuNCs. The optical properties of pap-AuNCs were characterized by UV-Vis absorption and fluorescence spectra. The surface plasmon resonance band is absent in the UV-Vis spectrum and intense emission in the visible region suggests the molecule-like properties of AuNCs and the lack of larger particles. [47] The developed nano-system exhibited the distinct characteristics fluorescence band at 670 nm and red fluorescent colour under UV light at 365 nm, indicating the successful formation of fluorescent gold nanoclusters (Fig. 1). Further, the DLS analysis of pap-AuNCs was performed to measure the nanocluster size. To measure DLS, 100 µL of pap-AuNCs from the stock was diluted to 2 mL with water. According to the DLS analysis, the average hydrodynamic size of pap-AuNCs was 17 nm (Fig. 2).

Interaction with VB_6 Cofactors

Pap-AuNCs' fluorescence response was investigated with various VB_6 cofactors. For this study, the probe was prepared by diluting 100 µL of pap-AuNCs with 1900 µL of water, followed by the recorded fluorescence spectrum showed the red-emitting fluorescent band at ~670 nm ($\lambda_{ex}=380$ nm). The selectivity of pap-AuNCs was explored by adding various VB_6 cofactors (PL, PN, PLP, and PYOA). To study the interaction, 100 µL of pap-AuNCs from the stock was taken and mixed with 100 µL of various VB_6 cofactors (1 mM) followed by diluted to 2 mL with double distilled water. The vials were gently shaken, and then the fluorescence spectra were recorded (Fig. 3). The emission band of pap-AuNCs was quenched, and a new band appeared for PLP. However, no observation in the fluorescence spectra and color of the AuNCs were noted by other VB_6 cofactors.

The addition of PLP altered the fluorescence emission of pap-AuNCs. Thus, fluorescence titration was carried out to assess the sensitivity. Incremental amounts of PLP (10 µL to 130 µL, 1 mM) were added to the pap-AuNC solution, and the spectra were recorded after each successive aliquot (10 µL) addition. The spectral changes showed the pap-AuNCs' fluorescence intensity dropped at 670 nm, together with the simultaneous enhancement at 525 nm (Fig. 5a). Red-emitting pap-AuNCs was changed into orange-emitting PLP_pap-AuNCs as a result of PLP addition. The bond formed between PLP's aldehyde group and the unbound amine groups of papain functionalized AuNCs resulted in

Fig. 2 The DLS image of pap-AuNCs

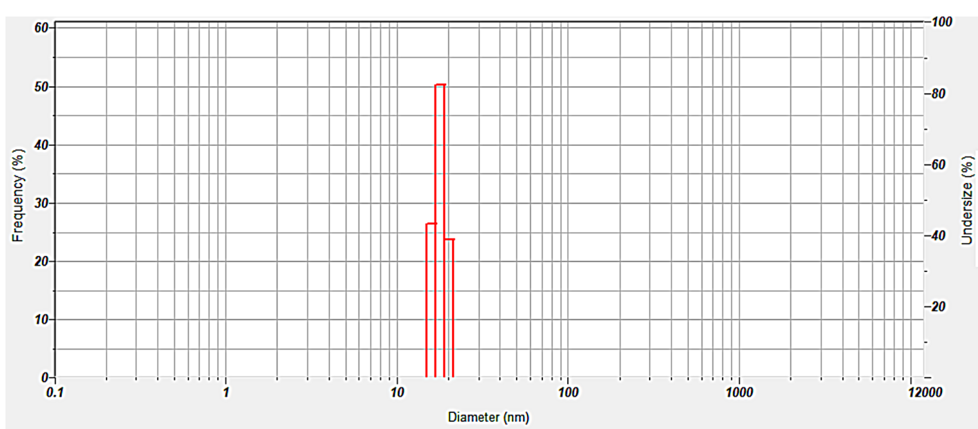

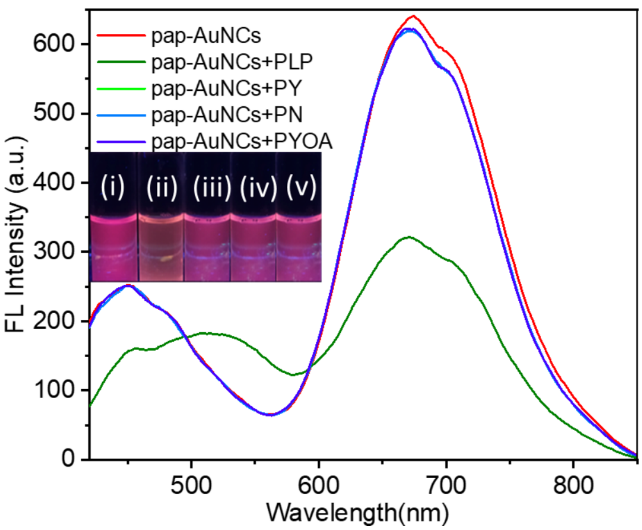

Fig. 3 Fluorescence spectral changes of pap-AuNCs in the presence of various VB_6 (inset shows the fluorescent colour changes of pap-AuNCs in the absence (i) and presence of PLP (ii), PY (iii), PN (iv), PYOA (v))

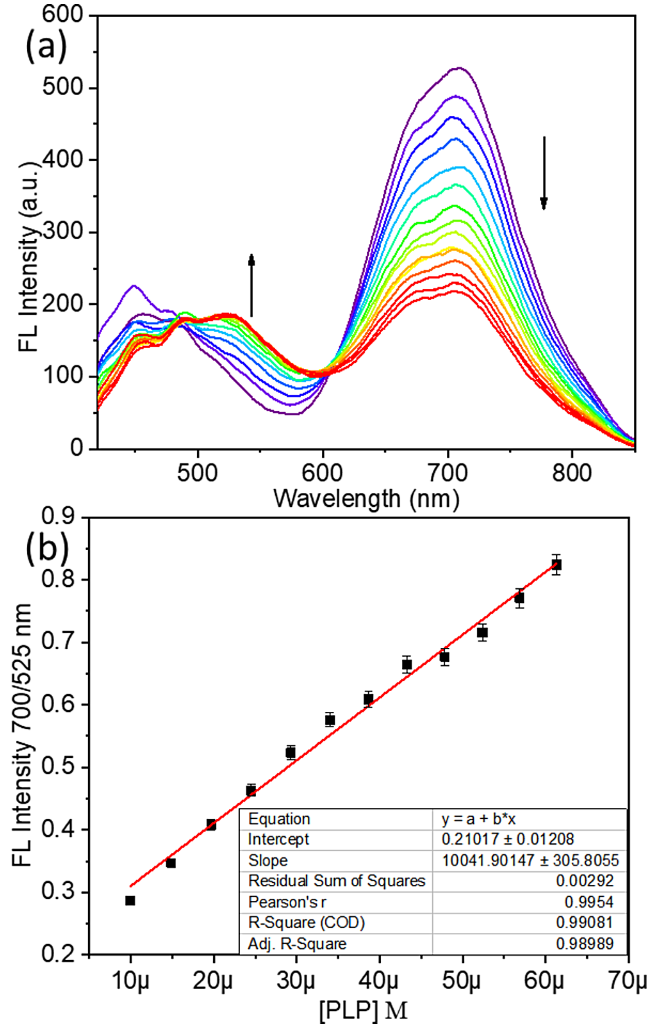

Fig. 5 (**a**) Fluorescence spectral changes of PLP-pap-AuNCs upon successive incremental addition of PLP (10 µL, 1 mM). (**b**) Calibration curves for the detection of PLP

the formation of a Schiff base over the nanoclusters surface, [48] which was responsible for the changes observed in the fluorescence spectra and color. The particles have a hydrodynamic size of approximately 59 nm, according to the DLS measurement of PLP_pap-AuNCs (Fig. 4). A plot was drawn by plotting of pap-AuNCs' ratiometric fluorescence spectral changes (700 nm/525 nm) against the added PLP concentrations. The calibration plot displays a good linearity with $R^2 = 0.9977$ between the concentration range of 10 µM to 65 µM (Fig. 5b). From the slope of the calibration plot, the detection limit was calculated as 0.59 µM.

Detection of Zn^{2+}

To detect metal ions, the PLP-conjugated nano-assembly PLP_pap-AuNCs was used as a nanoprobe. To create a 2 mL aqueous solution of the nanoprobe, 100 µL (1 mM) of PLP was combined with 100 µL of pap-AuNCs stock solution. Different metal ions (100 µL, 1 mM), such as Ni^{2+}, Ca^{2+}, Mg^{2+}, Cd^{2+}, Zn^{2+}, Cr^{3+}, Pb^{2+}, Mn^{2+}, Fe^{2+}, Fe^{3+}, Hg^{2+}, and Al^{3+} were introduced in aqueous medium to test the selectivity of the nanoprobe. Interestingly, Zn^{2+} significantly altered the fluorescence colour and profile of PLP_pap-AuNCs (Fig. 6). A 3-fold enhancement in the fluorescent intensity of PLP_pap-AuNCs was observed at 477 nm. Addition of Mg^{2+} and Mn^{2+} induced a very negligible (~0.3-fold) fluorescence enhancement at 477 nm, but other metal ions failed to enhance the fluorescence intensity of PLP_pap-AuNCs at 477 nm. When PLP_pap-AuNCs interacted with Zn^{2+}, their fluorescence showed a blue shift and increased at 477 nm. Additionally, PLP_pap-AuNCs'

Fig. 4 The DLS image of 2 mL solution of PLP_pap-AuNCs in water containing 100 µL of pap-AuNCs from the stock and 100 µL of PLP (1 mM)

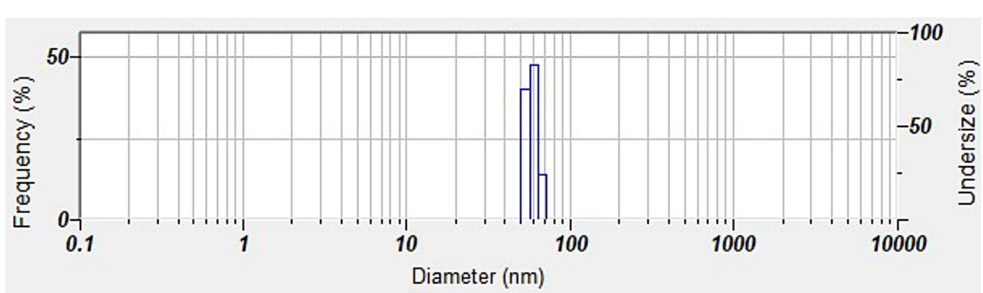

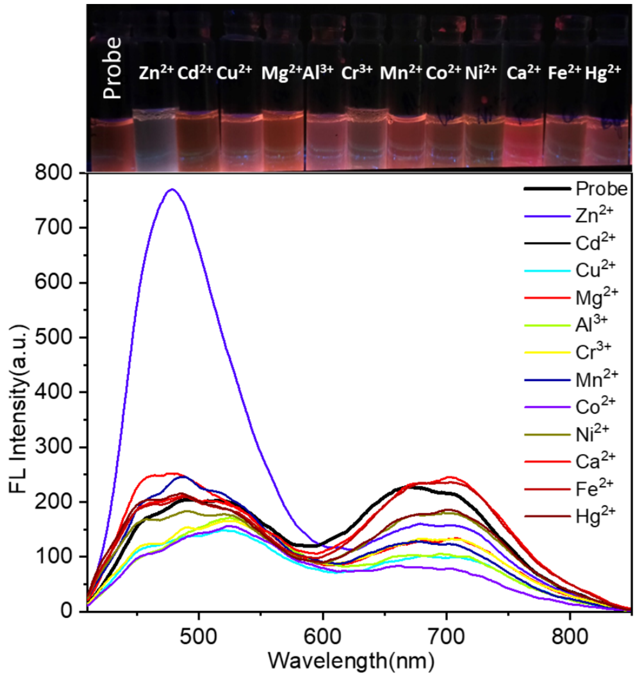

Fig. 6 Fluorescence spectral changes of probe PLP-pap-AuNCs in the presence of different metal cations (50 µM)

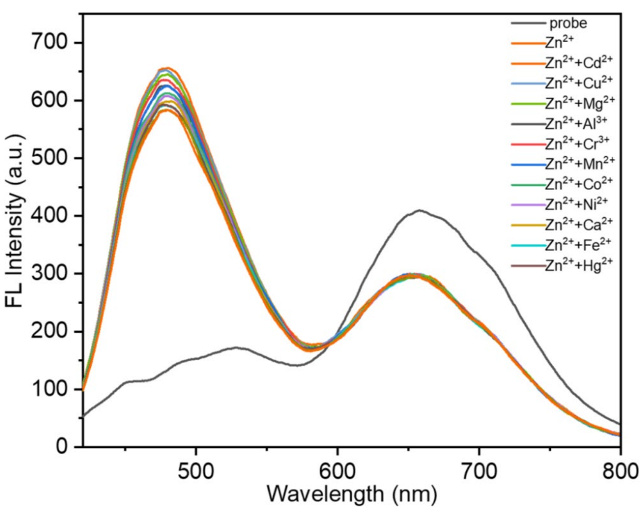

Fig. 7 The fluorescence spectral changes of PLP_pap-AuNCs (probe) in the presence of Zn^{2+} and equimolar amount of other interfering metal cations

fluorescence spectra were captured when Zn^{2+} and other interfering metal ions were present in equimolar concentrations (100 µL, 1 mM). Interestingly, the fluorescence enhancement at 477 nm of PLP_pap-AuNCs by Zn^{2+} alone was also observed in the co-presence of interfering metal ions. The recorded spectra in Fig. 7 revealed that a slight variation in the Zn^{2+} induced fluorescence enhancement of PLP_pap-AuNCs was observed when other tested interfering metal ions were present. These results validated

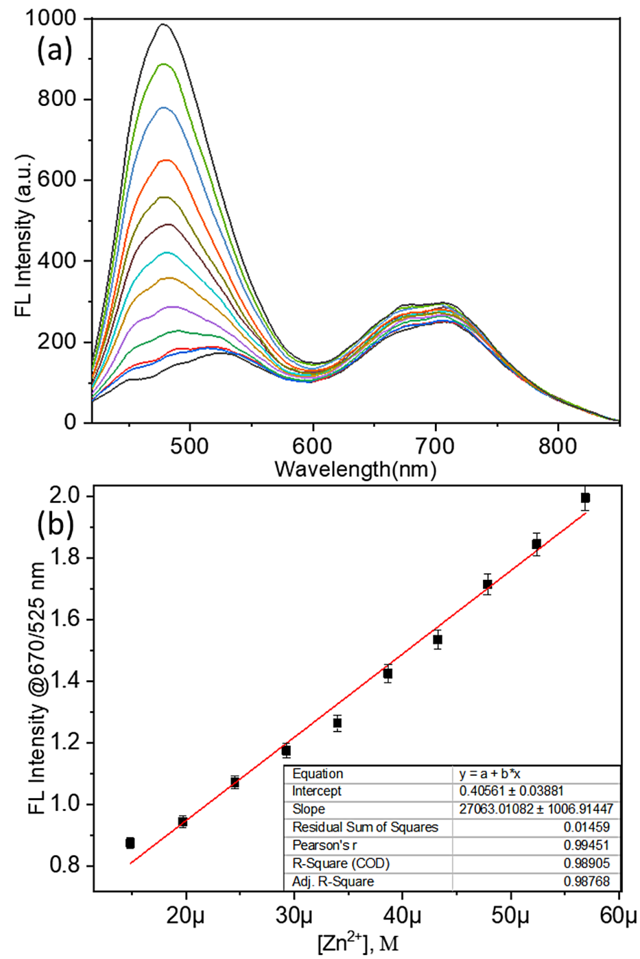

Fig. 8 (**a**) The fluorescence spectral changes of PLP_pap-AuNCs (probe) upon incremental addition of Zn^{2+} (10 µL, 1 mM). (**b**) Calibration curves for the PLP_pap-AuNCs@Zn^{2+}

the nanoprobe PLP_pap-AuNCs's exceptional Zn^{2+} ion selectivity.

Further, by adding different quantities of Zn^{2+}, fluorescence titration was used to test the sensitivity of PLP_pap-AuNCs as a Zn^{2+} nanoprobe (Fig. 8). Orange fluorescence emission was seen by the nanoprobe, with noticeable bands at 525 and 670 nm. As the Zn^{2+} amounts increased from 10 µL to 120 µL (1 mM), a gradual blue-shift from 525 nm and enhancement was observed at 477 nm. At 670 nm, no discernible alterations in the fluorescence spectrum were seen. Plotting the calibration curve against the added Zn^{2+} concentrations shows a good linear relationship for the fluorescence increase (Fig. 8b**)**, with values ranging from 14.7 µM to 56.9 µM and the detection limit computed down to 0.14 µM.

The average hydrodynamic diameter of PLP_pap-AuNCs increased from 59 nm to 97 nm following the addition of Zn^{2+}(Fig. 9). The interaction between Zn^{2+} and PLP_pap-AuNCs is suggested from the increase in the hydrodynamic

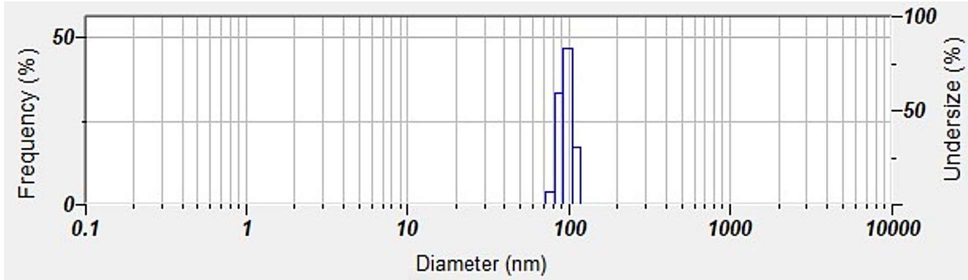

Fig. 9 The DLS image of 2 mL solution of PLP_Pap-AuNCs@ Zn^{2+} in water containing 100 μL of pap-AuNCs from the stock, PLP (100 μL, 1 mM) and Zn^{2+} (100 μL, 1 mM)

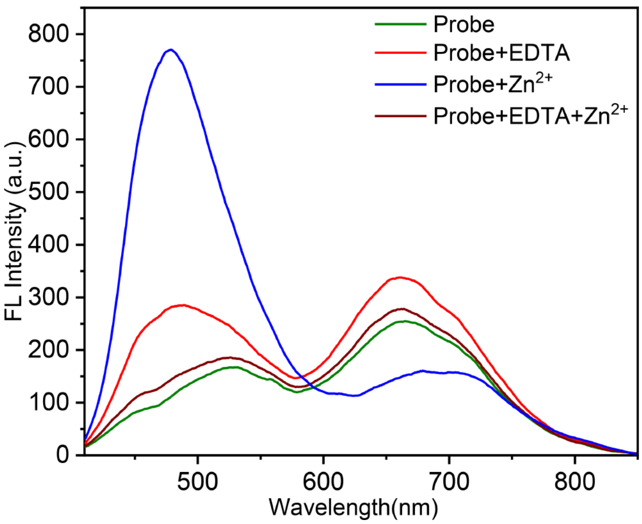

Fig. 10 Fluorescence spectra of PLP-pap-AuNCs in the absence and presence of Zn^{2+} and EDTA

Table 1 Results of real sample analysis of Zn^{2+} in tap water and river water

Samples	Zn^{2+}			RSD
	Added, [M]	Found, [M]	Recovery, (%)	
River water	1.48×10^{-5}	1.39×10^{-5}	94	1.92
	1.96×10^{-5}	1.89×10^{-5}	96	1.28
Tap water	1.48×10^{-5}	1.46×10^{-5}	99	0.58
	1.96×10^{-5}	1.80×10^{-5}	91	2.31

diameter. With two donor atoms (phenolic-OH and imine-N) on the surface of PLP_pap-AuNCs due to PLP conjugation offers an optimal coordination environment that facilitates Zn^{2+} recognition and modifies fluorescence as a result of internal charge transfer from ligand to metal (LMCT). EDTA, a potent chelating agent, was added to PLP_pap-AuNCs' surface to verify the complexation of Zn^{2+}. When EDTA was added, the increased fluorescence emission of PLP_pap-AuNCs at 477 nm caused by Zn^{2+} was reversed. This reversal happened as a result of the strong complexing activity of EDTA, which is predicted to decomplex Zn^{2+} and restore PLP_pap-AuNCs' fluorescence emission (Fig. 10).

Overall, the detection of Zn^{2+} by PLP_pap-AuNCs is schematically presented in Scheme 1. The red-emitting pap-AuNCs interacted with PLP by forming an imine linkage and changed the fluorescent colour from red to orange. The Schiff base formation over the surface of the nanoclusters provide an ideal coordination environment to chelate Zn^{2+}. When Zn^{2+} is added to the PLP_pap-AuNCs, the fluorescent emission enhanced at 477 nm due to the complexation-induced aggregation of PLP_pap-AuNCs. The aggregation of PLP_pap-AuNCs was supported by DLS, whereas the complexation-induced aggregation was complemented by reversibility experiment performed by adding strong chelating agent EDTA.

Real Sample Analysis

Zn^{2+} measurement was done in environmental water samples to show the applicability of PLP_pap-AuNCs. To get rid of big particles, the collected water samples were first filtered. These samples were then added to the PLP_pap-AuNCs solution and spiked with known concentrations of Zn^{2+}. The calibration curve was used to calculate the Zn^{2+} concentration after the fluorescence spectra were recorded. Table 1 presents a summary of the acquired results, which indicate recoveries between 91% and 99%, with a maximum standard deviation (RSD) of roughly 3%. These results demonstrate the PLP_pap-AuNCs nanoprobe's potential for measuring Zn^{2+} in actual environmental water samples.

The paper strips and cotton buds coated with pap-AuNCs and PLP_pap-AuNCs were prepared and shown in Fig. 11. The developed paper strips and cotton buds displayed the fluorescent colour of the respective nanoclusters, i.e., (i) pap-AuNCs, (ii) PLP_pap-AuNCs, and (iii) PLP_pap-AuNCs in the presence of Zn^{2+} ions. The nanoprobe PLP_pap-AuNCs paper strips and cotton buds also showed visual fluorescent colour changes in the presence of Zn^{2+}. Thus, the created a nanoprobe PLP_pap-AuNCs can also be used to visually detect Zn^{2+} ions.

Conclusions

In summary, the nanocluster emitting red-fluorescent pap-AuNCs was employed for the cascade detection of two important biospecies PLP and Zn^{2+} in a straightforward and

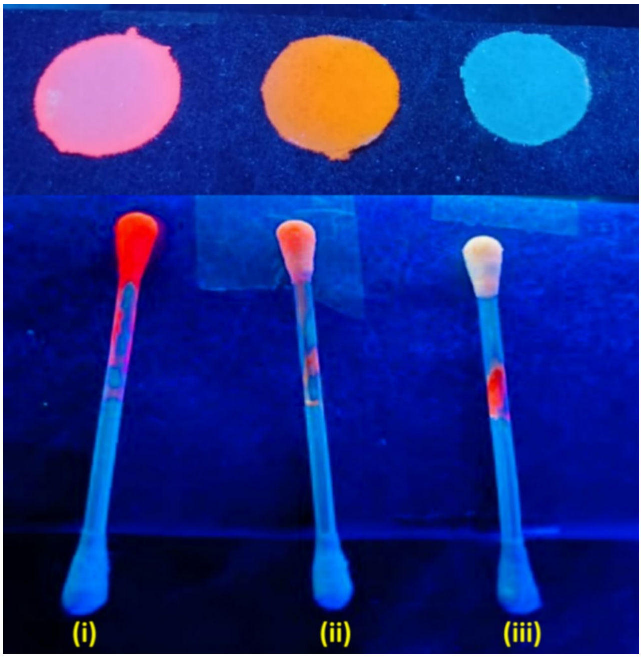

Fig. 11 Paper strips and cotton buds coated with (i) pap-AuNCs, (ii) PLP_pap-AuNCs, and (iii) PLP_pap-AuNCs in the presence of Zn^{2+} ions

cost-effective manner. The interaction between PLP and papain-functionalized AuNCs leads to a noticeable change in the nanocluster's emission, which allowed the detection of vitamin B_6 cofactor i.e. PLP down to 0.59 µM. The added PLP is expected to form imine linkage with the free $-NH_2$ groups of papain stabilized over pap-AuNCs and form the PLP conjugated nanoclusters PLP_pap-AuNCs. Further addition of Zn^{2+} ions to the solution of PLP_pap-AuNCs resulted in a significant fluorescent enhancement at 477 nm due to the complexation-induced aggregation of PLP_pap-AuNCs. PLP_pap-AuNCs can be used to detect Zn^{2+} ions down to 0.14 µM. The Zn^{2+} ions detection conducted in actual water samples proved the analytical usefulness of PLP_pap-AuNCs.

Acknowledgements Not applicable.

Author Contributions All authors contributed to the study. The Investigation, Validation, Formal analysis, Data curation, Writing-original draft were performed by Jayant Chaudhary and Aditi Tripathi. The Conceptualization, Resources, Supervision, and Writing-review & editing were performed by Suban K Sahoo.

Funding Not applicable.

Data Availability No datasets were generated or analysed during the current study.

Declarations

Ethical Approval Not applicable as the study does not include any use of animals and humans.

Consent to Publish Not applicable.

Consent to Participate Not applicable.

Competing Interests The authors declare no competing interests.

References

1. Rajamanikandan R, Sasikumar K, Kosame S, Ju H (2023) Optical sensing of toxic cyanide anions using Noble Metal nanomaterials. Nanomaterials 13:290
2. Rajamanikandan R, Shanmugaraj K, Ilanchelian M, Ju H (2023) Cysteamine-decorated gold nanoparticles for plasmon-based colorimetric on-site sensors for detecting cyanide ions using the smart-phone color ratio and for catalytic reduction of 4-nitrophenol. Chemosphere 316:137836
3. Rajamanikandan R, Ilanchelian M, Ju H (2023) Highly selective uricase-based quantification of Uric Acid using hydrogen peroxide sensitive Poly-(vinylpyrrolidone) templated copper nanoclusters as a fluorescence probe. Chemosensors 11:268
4. Dash PP, Ghosh AK, Mohanty P, Behura R, Behera S, Jali BR, Sahoo SK (2024) Advances on fluorescence chemosensors for selective detection of water. Talanta 275:126089
5. Zhang L, Wang E (2014) Metal nanoclusters: new fluorescent probes for sensors and bioimaging. Nano Today 9(1):132–157
6. Sahoo SK, Sharma D, Bera RK, Crisponi G, Callan JF (2012) Iron(III) selective molecular and supramolecular fluorescent probes. Chem Soc Rev 41(21):7195–7227
7. Sahoo SK, Kim G-D, Choi H-J (2016) Optical sensing of anions using C3v-symmetric tripodal receptors. J Photochem Photobiol C: Photochem 27:30–53
8. Valeur B, Leray I (2000) Design principles of fluorescent molecular sensors for cation recognition. Coord Chem Rev 205(1):3–40
9. Zhang J, Campbell RE, Ting AY, Tsien RY (2002) Creating new fluorescent probes for cell biology. Nat Rev Mol Cell Biol 3(12):906–918
10. Prasad AS (2009) Zinc: role in immunity, oxidative stress and chronic inflammation. Curr Opin Clin Nutr Metabolic Care 12(6):646–652
11. Shankar AH, Prasad AS (1998) Zinc and immune function: the biological basis of altered resistance to infection. Am J Clin Nutr 68(2):447S–463S
12. Pastorekova S, Parkkila S, Pastorek J, Supuran CT (2004) Review article. J Enzyme Inhib Med Chem 19(3):199–229
13. Reid MF, Fewson CA (1994) Molecular characterization of microbial alcohol dehydrogenases. Crit Rev Microbiol 20(1):13–56
14. Sandstead HH (1994) Understanding zinc: recent observations and interpretations. J Lab Clin Med 124(3):322–327
15. Arthur B, Chausmer S (1998) Zinc, insulin and diabetes. J Am Coll Nutri 17(2):109–115
16. Ghosh SK, Kim P, Zhang X-a, Yun S-H, Moore A, Lippard SJ, Medarova Z (2010) A novel imaging approach for early detection of prostate cancer based on endogenous zinc sensing. Cancer Res 70(15):6119–6127
17. Dean KM, Qin Y, Palmer AE (2012) Visualizing metal ions in cells: an overview of analytical techniques, approaches, and probes. Biochim et Biophys Acta (BBA)-Molecular Cell Res 1823(9):1406–1415

18. Pluth MD, Tomat E, Lippard SJ (2011) Biochemistry of mobile zinc and nitric oxide revealed by fluorescent sensors. Annu Rev Biochem 80:333–355
19. Duan X, Sun R, Fang J (2017) On-line continuous generation of zinc chelates in the vapor phase by reaction with sodium dithiocarbamates and determination by atomic fluorescence spectrometry. Spectrochimica Acta Part B: at Spectrosc 128:11–16
20. Binet MR, Ma R, McLeod CW, Poole RK (2003) Detection and characterization of zinc-and cadmium-binding proteins in Escherichia coli by gel electrophoresis and laser ablation-inductively coupled plasma-mass spectrometry. Anal Biochem 318(1):30–38
21. Dueraning A, Kanatharana P, Thavarungkul P, Limbut W (2016) An environmental friendly electrode and extended cathodic potential window for anodic stripping voltammetry of zinc detection. Electrochim Acta 221:133–143
22. Xu Z, Yoon J, Spring DR (2010) Fluorescent chemosensors for Zn(2+). Chem Soc Rev 39:1996–2006
23. Sahoo SK (2021) Chromo-fluorogenic sensing using vitamin B6 cofactors and derivatives: a review. New J Chem 45:8874–8897
24. Fogle EJ, Liu W, Woon S-T, Keller JW, Toney MD (2005) Role of Q52 in catalysis of decarboxylation and transamination in dialkylglycine decarboxylase. Biochemistry 44(50):16392–16404
25. Sun S, Toney MD (1999) Evidence for a two-base mechanism involving tyrosine-265 from arginine-219 mutants of alanine racemase. Biochemistry 38(13):4058–4065
26. Du Y-L, Ryan KS (2019) Pyridoxal phosphate-dependent reactions in the biosynthesis of natural products. Nat Prod Rep 36(3):430–457
27. Eliot AC, Kirsch JF (2004) Pyridoxal phosphate enzymes: mechanistic, structural, and evolutionary considerations. Annu Rev Biochem 73(1):383–415
28. Toney MD (2005) Reaction specificity in pyridoxal phosphate enzymes. Arch Biochem Biophys 433(1):279–287
29. Schneider G, Käck H, Lindqvist Y (2000) The manifold of vitamin B6 dependent enzymes. Structure 8(1):R1–R6
30. Parra M, Stahl S, Hellmann H (2018) Vitamin B6 and its role in cell metabolism and physiology. Cells 7(7):84
31. Ueland PM, Ulvik A, Rios-Avila L, Midttun Ø, Gregory JF (2015) Direct and functional biomarkers of vitamin B6 status. Annu Rev Nutr 35:33–70
32. Thiamin R (1998) Dietary reference intakes for Thiamin, Riboflavin, Niacin, vitamin B6, folate, vitamin B12, pantothenic acid, biotin, and Choline1. National Academies Press (US), Washington (DC)
33. Merete C, Falcon LM, Tucker KL (2008) Vitamin B6 is associated with depressive symptomatology in Massachusetts elders. J Am Coll Nutr 27(3):421–427
34. Malouf R, Evans JG (2003) The effect of vitamin B6 for cognition. Cochrane Database Syst Reviews (4), CD004393
35. Qian B, Shen S, Zhang J, Jing P (2017) Effects of vitamin B6 deficiency on the composition and functional potential of T cell populations. J Immunol Res 2017:2197975
36. Ueland PM, McCann A, Midttun Ø, Ulvik A (2017) Inflammation, vitamin B6 and related pathways. Mol Aspects Med 53:10–27
37. Scott K, Zeris S, Kothari MJ (2008) Elevated B6 levels and peripheral neuropathies. Electromyogr Clin Neurophysiol 48(5):219–223
38. Clayton PT (2006) B6-responsive disorders: a model of vitamin dependency. J Inherit Metab Dis 29(2):317–326
39. Hyotanishi M, Isomura Y, Yamamoto H, Kawasaki H, Obora Y (2011) Surfactant-free synthesis of palladium nanoclusters for their use in catalytic cross-coupling reactions. Chem Commun 47(20):5750–5752
40. Bhardwaj V, Anand T, Choi H-J, Sahoo SK (2019) Sensing of Zn(II) and nitroaromatics using salicyclaldehyde conjugated lysozyme-stabilized fluorescent gold nanoclusters. Microchem J 151:104227
41. Xie J, Zheng Y, Ying JY (2009) Protein-directed synthesis of highly fluorescent gold nanoclusters. J Am Chem Soc 131(3):888–889
42. Chang H-C, Chang Y-F, Fan N-C, Ho J-aA, Interfaces (2014) Facile preparation of high-quantum-yield gold nanoclusters: application to probing mercuric ions and biothiols. ACS Appl Mater Interfaces 6(21):18824–18831
43. Pramanik G, Humpolickova J, Valenta J, Kundu P, Bals S, Bour P, Dracinsky M, Cigler P (2018) Gold nanoclusters with bright near-infrared photoluminescence. Nanoscale 10(8):3792–3798
44. Wu Z, Jin R (2010) On the ligand's role in the fluorescence of gold nanoclusters. Nano Lett 10(7):2568–2573
45. Chen Y, Qiao J, Liu Q, Zhang M, Qi L (2018) Fluorescence turn-on assay for detection of serum D-penicillamine based on papain@ AuNCs-Cu2 + complex. Anal Chim Acta 1026:133–139
46. Tripathi A, Ghosh AK, Sahoo SK (2024) Smartphone-assisted cost-effective approach for detecting mercury(II) using papain stabilized fluorescent gold nanoclusters. Inorg Chim Acta 567:122059
47. Hambarde G, Bothra S, Upadhyay Y, Bera RK, Sahoo SK (2019) m-Dinitrobenzene directed aggregation-induced emission enhancement of cysteine modified fluorescent copper nanoclusters. Microchem J 147:899–904
48. Nakum R, Ghosh AK, Jali BR, Sahoo SK (2024) Fluorescent ovalbumin-functionalized gold nanocluster as a highly sensitive and selective sensor for relay detection of salicylaldehyde, Hg(II) and folic acid. Spectrochim Acta A 313:124143

Publisher's Note Springer Nature remains neutral with regard to jurisdictional claims in published maps and institutional affiliations.

Springer Nature or its licensor (e.g. a society or other partner) holds exclusive rights to this article under a publishing agreement with the author(s) or other rightsholder(s); author self-archiving of the accepted manuscript version of this article is solely governed by the terms of such publishing agreement and applicable law.